AD-A041 445 WASHINGTON UNIV SEATTLE DEPT OF MECHANICAL ENGINEERING F/G 20/11
A PROCEDURE FOR EVALUATING FRACTURE DYNAMIC PARAMETERS FROM CRA--ETC(U)
MAY 77 A S KOBAYASHI, S MALL N00014-76-C-0060

UNCLASSIFIED TR-28 NL

| OF |
AD
A041445

END

DATE
FILMED
8-77

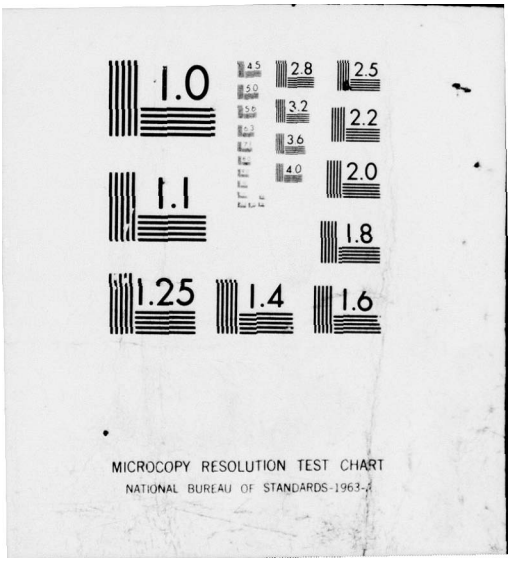
1.0
1.1
1.25
1.4
1.6
1.8
2.0
2.2
2.5
2.8
3.2
3.6
4.0
4.5
5.0
5.6
MICROCOPY RESOLUTION TEST CHART
NATIONAL BUREAU OF STANDARDS-1963-A

Office of Naval Research

Contract N00014-76-C-0060 NR 064-478

Technical Report No. 28

A PROCEDURE FOR EVALUATING FRACTURE DYNAMIC PARAMETERS FROM CRACK VELOCITY MEASUREMENTS

by

A.S. Kobayashi and S. Mall

May 1977

The research reported in this technical report was made possible through support extended to the Department of Mechanical Engineering, University of Washington, by the Office of Naval Research under Contract N00014-76-C-0060 NR 064-478. Reproduction in whole or in part is permitted for any purpose of the United States Government.

Department of Mechanical Engineering

College of Engineering

University of Washington

400 314

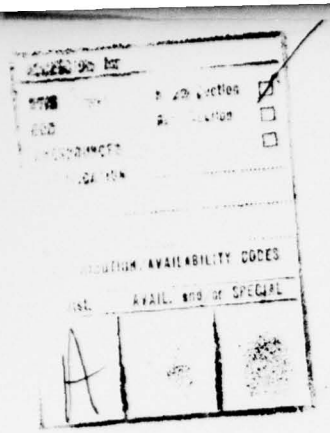

A PROCEDURE FOR EVALUATING FRACTURE DYNAMIC PARAMETERS FROM CRACK VELOCITY MEASUREMENTS

A. S. Kobayashi and S. Mall

Department of Mechanical Engineering, University of Washington

ABSTRACT

A combined numerical and experimental procedure for evaluating some of the fracture dynamic parameters which govern the crack run-arrest response in a fracturing plate are discussed. A dynamic finite element code is used to compute the dynamic stress intensity factor and dynamic energy release rate associated with a propagating crack which is driven by the experimentally determined crack velocity. Numerical results generated by the developed procedure are then compared with dynamic stress intensity factors obtained through dynamic photoelastic analyses of fracturing Homalite-100 plates. Two edge-cracked specimens with fixed edge displacement loadings and two wedge-loaded double cantilever beam specimens were considered in this comparative study. Good agreements were obtained between the results obtained by the developed numerical-experimental procedure and dynamic photoelasticity.

INTRODUCTION

The three approaches currently in use in fracture dynamic studies are: to relate the experimentally determined crack velocities with static fracture parameters [1]; to relate experimentally determined crack velocities with those obtained from an analytical dynamic model without or with postulated dynamic fracture toughness [2,3,4]; and to determine experimentally the dynamic state of stress in fracturing polymeric materials [5,6,7]. In this paper, a fourth procedure, which utilizes the versatility of dynamic finite element method (FEM) to extract fracture dynamic parameters from the most commonly measured quantity of crack velocity in practical structural material is described. The procedure is then used to indicate the errors involved in using static analysis to interpret dynamic results.

DYNAMIC FINITE ELEMENT CODE

The dynamic finite element method (FEM) which has evolved since its initial use [8] in this combined numerical-experimental procedure is the FEM

code HONDO [9] with artificial viscosity to reduce the keystoning effect in the finite elements along the opening crack surfaces. In this dynamic FEM procedure, crack extension is modeled by discontinuous jumps of the crack tip from one finite element node to its adjacent node and the time-averaged crack tip displacement is equated to the average crack tip velocity at the adjacent node. The average work necessary to open the newly created increment of crack surface is then used to compute the surface energy dissipation rate which is equated to the dynamic energy release rate at the crack tip node just prior to the subsequent discrete movement of the crack tip [8]. An accuracy check of this direct procedure for computing the dynamic energy release rate was established by a comparative study with Baker's solution [10] where the numerical and theoretical results agreed within 1 percent of each other [8].

More recently another check on the dynamic finite element algorithm was made by comparing the crack opening displacements (COD) of a constant velocity crack against the theoretical solution of Broberg [11]. In this numerical study involving a fracturing steel plate, an artificial keystone viscosity of B3=0.2 was used to damp out the keystoning effect prevalent in previous analyses. The numerically determined time-averaged COD at every other node away from the moving crack tip was found to be in excellent agreement with Broberg's result for a crack velocity of $c/c_1 = 0.076$ where c and c_1 are the crack and dilatational wave velocities, respectively [12]. It was also shown that at this low crack velocity, the stress intensity factor computed by static near field solution was only 2.2 percent higher than that computed by the dynamic near field solution when dynamic finite element COD values were used to compute the dynamic stress intensity factor.

In order to examine further the effectiveness of the above COD technique in dynamic finite element analysis of fracturing Homalite-100 plates, the well analyzed fracturing dynamic photoelastic specimens B2 and B13 [8] were reanalyzed with various artificial viscosities. The finite element breakdown and the crack velocities used in this new study are identical to those used in Reference [8]. Figure 1 shows the crack opening displacements at three crack lengths in Specimen B2 with three artificial viscosities. The small artificial viscosity of B3 = 0.01 and 0.1 were not very effective in removing keystoning but the prominent fluctuations in COD were substantially suppressed with B3 = 0.5. It should also be noted that a significant change was made in the numerical algorithm where the initial residual surface tractions along crack propagation were computed by using a static modulus of elasticity of E_S = 540 ksi while all stress wave propagation induced by the running crack were computed with a dynamic modulus of elasticity of E_D = 675 ksi. This combined use of static and dynamic moduli of elasticity in dynamic finite element analysis, initially proposed by Gehlen [13], is an attempt to model the strain rate sensitivity of the modulus of elasticity of Homalite-100 material. Such strain rate sensitivity did not exist in the fracture dynamic analysis of steel tapered DCB specimen [12] which is easier to analyze by dynamic finite element analysis than the photoelastic specimens. Our continuing interest in using dynamic photoelasticity to study fracture dynamics despite the added complexity of strain rate sensitivity

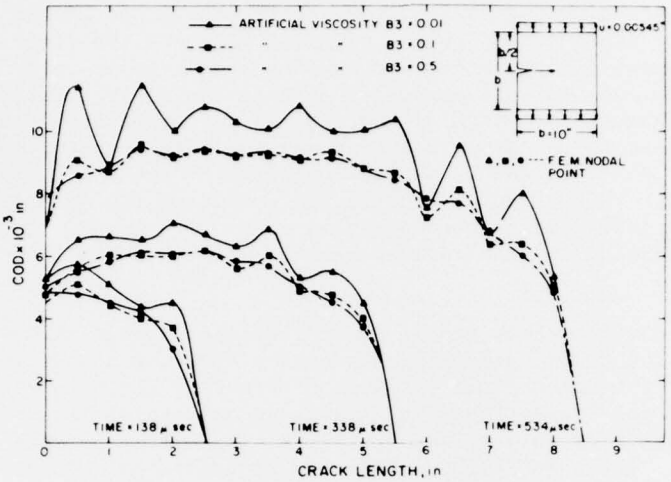

Fig. (1) - Effect of artificial keystone viscosity on COD in Test No. B2.

stems from the fact that no other experimental technique can provide an accurate near field state of stress in the vicinity of a running crack. Dynamic photoelasticity is one of few optical techniques which can provide experimentally determined dynamic stress intensity factor with which our numerical results could be compared. As will be shown later, such dynamic stress intensity factors computed through the combined use of static and dynamic moduli of elasticity agreed well with the experimental results under the state of plane strain. The latter state of plane strain for thicker Homalite-100 plates is considered to be a better modeling of the cleavage fractured surface observed in the fractured specimens.

Figure 2 shows the variations in dynamic stress intensity factors obtained numerically by the energy release rate method [8] and COD method [12] as well as their experimental counterpart determined by dynamic photoelasticity for Specimen B2. While the two numerical algorithms of computing dynamic stress intensity factors do not yield substantially different results, the more pronounced fluctuation in dynamic stress intensity factors computed by the COD method is noted. Thus this comparison favors the energy release rate procedure.

Likewise comparison is shown in Figure 3 for Specimen B13 in which the crack arrested. While the prominent peak in the experimentally determined dynamic stress intensity factor was not observed in the two numerical values, the experimental and numerical results are otherwise in good agreement with each other. Again the numerical results obtained by energy release rate procedure appears to be in slightly better agreement with the experimental results.

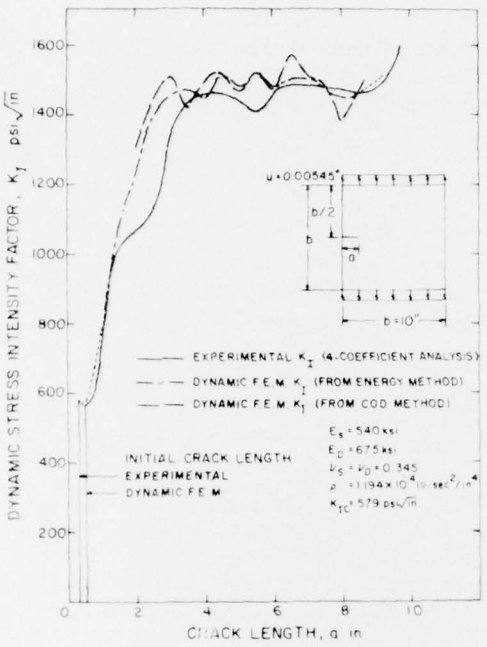

Fig. (2) - Dynamic stress intensity factors in Test No. B2, plane strain analysis

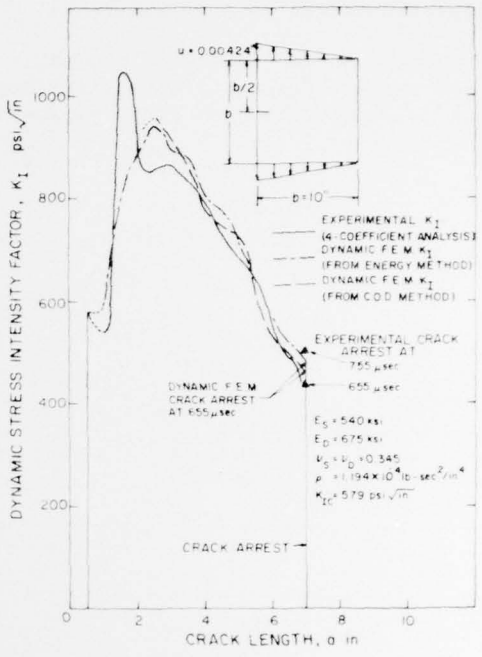

Fig. (3) - Dynamic stress intensity factors in Test No. B13, plane strain analysis

As a result of these two comparative studies using the well analyzed specimens B2 and B13, it was concluded that the energy release rate procedure provided slightly better numerical results of the fracturing Homalite-100 plates. This conclusion unfortunately differs with that in Reference [12] and is perhaps indicative of the larger keystoning effect in the Homalite-100 plates due to its much smaller modulus of elasticity.

WEDGE-LOADED DCB SPECIMEN

The above dynamic finite element algorithm was then used to analyze the dynamic crack arrest results of two wedge-loaded double cantilever beam (DCB) specimens machined from Homalite-100 plates of 1/2 inch nominal thickness [14]. The dynamic stress intensity factors of these two fracturing tapered DCB specimens were determined by a different data reduction scheme of dynamic photoelasticity results than that used by the authors [7]. The static and dynamic material properties as well as the crack position versus time relations reported in Reference [14] were used as input conditions to

our dynamic finite element analysis.

Figure 4 shows the finite element breakdown of one of the two tapered DCB specimens. Figures 5(a) and (b) show the crack position versus time relations which were used to propagate the crack tip intermittently along

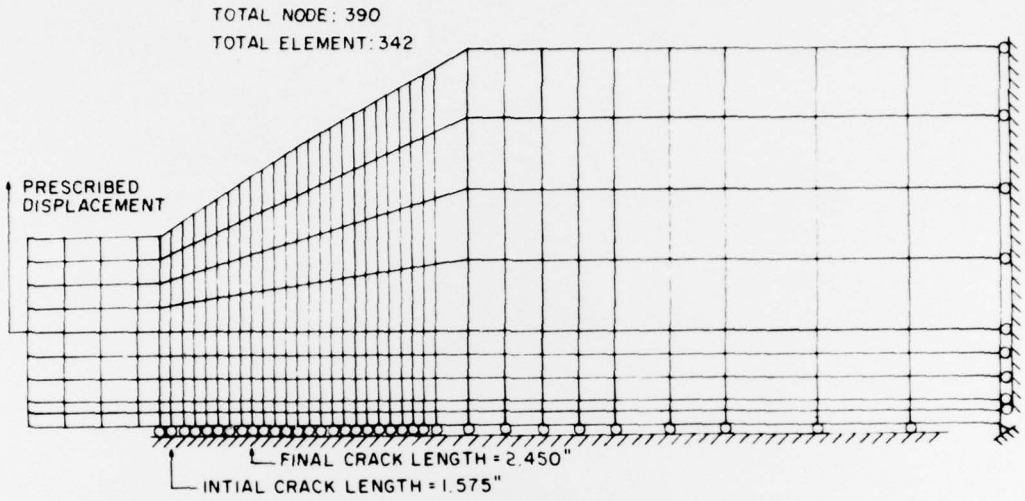

Fig. (4) - Finite element breakdown of wedge-loaded C-DCB model No. 7 [14]

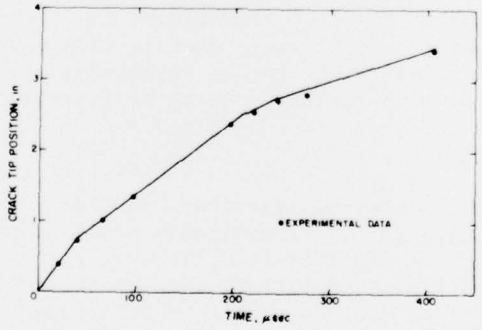

Fig. 5(a) - Crack tip position versus time in C-DCB model No. 6 [14]

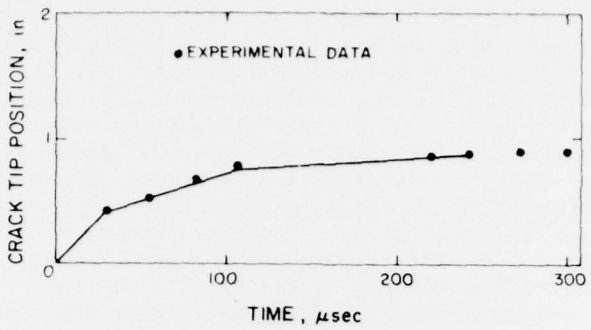

Fig. 5(b) - Crack tip position versus time in C-DCB model No. 7 [14]

the finite element nodes at prescribed time intervals. Fixed pin displacements were prescribed during the entire fracture process which were 459 and 300 microseconds for Specimens C-DCB Model Nos. 6 and 7, respectively. This assumption of fixed grip condition has been the source of discussion since one of the authors presented a dynamic finite element analysis of the crack propagation and arrest in a tapered DCB specimen using measured crack velocities [15]. The static stress intensity factor at crack arrest computed under the assumption of fixed grip condition was approximately 40 percent lower than the corresponding value computed under the assumption of variable load condition of Reference [16], thus indicating the sensitivity of the arrest stress intensity factor to the prescribed boundary condition during crack propagation in such small crack arrest specimen. Subsequent analysis of another tapered DCB specimen under the two different loading conditions of our fixed grip loading and the variable loading condition prescribed in References [16] and [17] showed that while the dynamic strains computed under the former condition agreed well with the three strain gage measurements [16], the corresponding dynamic strains computed under the assumption of variable loading differed considerably with experimental results [12]. As a result of this analysis [12], the fixed grip condition is believed to be a valid assumption in the series of experiments reported in Reference [16]. This conclusion also indicates that the crack arrest stress intensity factor determined by the procedure described in References [16] and [17] could grossly overestimate the crack arrest potential of the material tested.

Unfortunately, the excellent agreements between the crack arrest stress intensity factors determined by simulations of the crack arrest experiments of References [16] and [17] using Homalite-100 specimens [14] and the crack arrest stress intensity factors determined independently by dynamic photoelasticity [5] have been used as experimental evidence for justifying the variable pin loading in References [16] and [17]. A cursory study, however,

shows considerable differences between the relative compliances between the loading fixture and the Homalite-100 specimen in the dynamic photoelasticity experiments and those of References [16] and [17]. As a result, one can conclude qualitatively that the variable pin loads measured in the rigid loading fixture of the simulated experiments using Homalite-100 specimens should be closer to the pin loads obtained under fixed grip condition while such condition cannot be realized in the actual experiments using steel specimen. An experimental check in these relative compliances can be easily made to verify such hypothesis. Another procedure is to analyze numerically the fracture dynamic response of the Homalite-100 specimens following the procedure described in Reference [15] and then identify the differences or similarities between these results with those of Reference [12]. Dynamic finite element analyses under the fixed grip condition should thus provide this insight into the controversy surrounding the exact boundary conditions on the tapered DCB specimens used in crack arrest experiments.

Figure 6 shows the dynamic and static stress intensity factors obtained by static and dynamic finite element analyses under the assumption of fixed grip condition for a Homalite-100 C-DCB Model No. 6 [14]. Also shown are

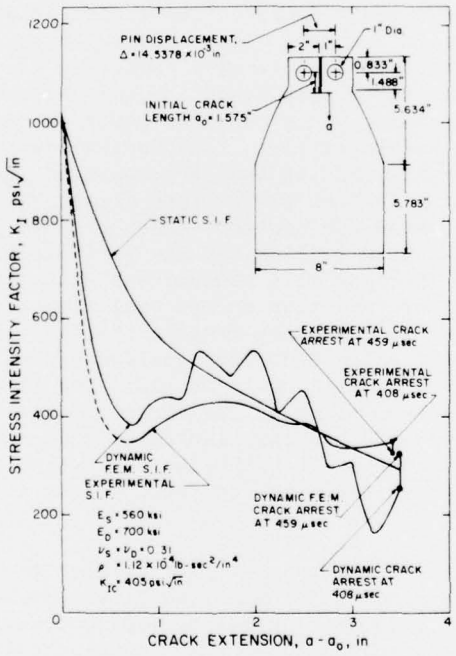

Fig. (6) - Stress intensity factors in a wedge-loaded contoured DCB specimen (Model No. 6). Load at fracture initiation = 151 lb [14].

the dyramic stress intensity factors of this specimen obtained by dynamic photoelasticity [14]. While the numerically obtained dynamic stress intensity factors show some small oscillations, the two results are generally in qualitative agreement with each other and in particular are in excellent agreement at crack arrest.

Figure 7 shows the crack opening displacements (COD) of the same specimen. As expected, the keystoning effect continues to increase with

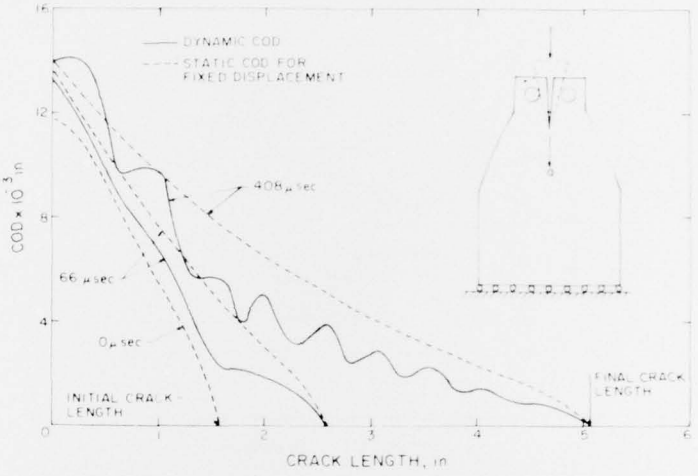

Fig. (7) - Crack opening displacement (COD) at different times in C-DCB Model No. 6 [14]

increase in crack length despite the high artificial viscosity of B3 = 0.5. The pronounced smaller dynamic crack opening displacements, which was also observed in the metallic specimens [12,15], in this cantilever beam type specimen are indications of the delayed response of the propagating crack tip to the applied load at the loading pin. Such delay response further verifies our assumed fixed grip loading condition during crack propagation and arrest.

Figure 8 shows the dynamic and static stress intensity factors in Specimen C-DCB Model No. 7. Again, relatively good agreement, particularly at crack arrest, between the experimental and numerical results is noted. The rapid small oscillations in dynamic stress intensity factors, which were noted in Figure 6, are absent in Figure 8. Our past experiences in numerical fracture dynamic analyses [4, 12] indicate that smoothed crack velocities generally result in oscillations in dynamic stress intensity factors and vice versa. Since the test results of Model C-DCB No. 6 recorded 9 crack positions for a crack extension of 3.41 in. while 7 crack positions are

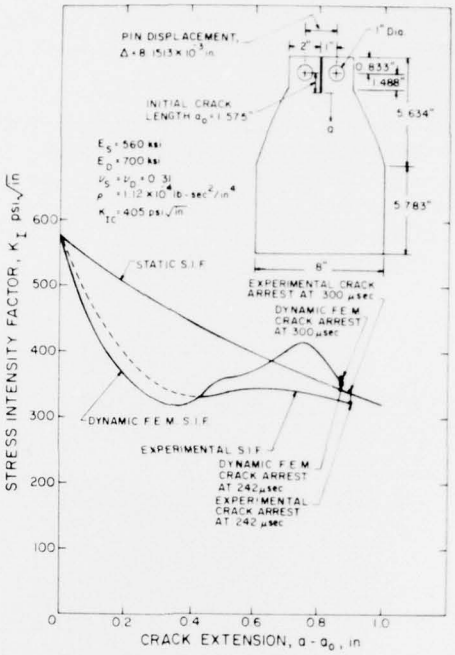

Fig. (8) - Stress intensity factors in a wedge-loaded contoured DCB specimen (Model No. 7). Load at fracture initiation = 89 lb [14].

recorded for a crack extension of 0.90 in. for Model 7, one would expect the crack position versus time relation for the test of Model 6 to represent a smoother time average position instead of a more precise crack position versus time relation necessary to generate a smoothly varying dynamic stress intensity as was the case of Model No. 7 test. Thus Model No. 7 should yield smoother variations in numerically computed dynamic stress intensity factor than Model No. 6.

The above good agreement between the variations in dynamic stress intensity factors with crack propagation obtained numerically and experimentally verifies the validity of the fixed grip condition under which the dynamic stress intensity factors were computed. Although the numerical results provide the variations in pin loads with respect to crack propagation as shown in Figure 9, corresponding experimental results were not available for direct comparison. Thus experimentally measured pin load from a separate test [14] is shown in Figure 9 for qualitative comparison. The two-fold differences between ringing frequencies of the numerical and experimental pin loads could be due to unavoidable compliance of the loading frame and

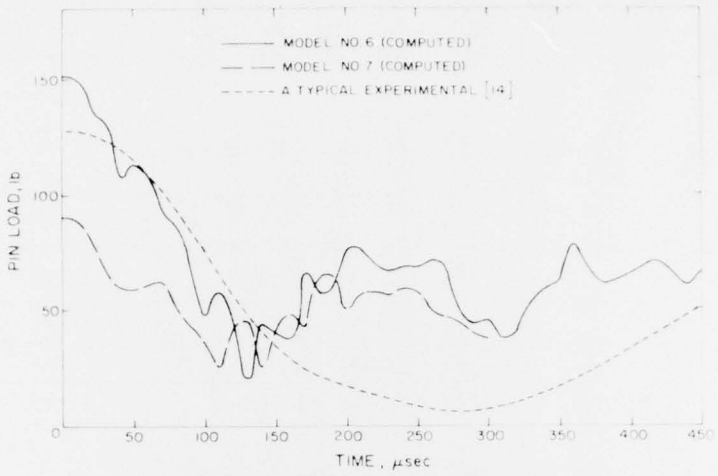

Fig. (9) - Pin load versus time in wedge-loaded C-DCB specimens

load cell system in the actual experimental setup.

DISCUSSION

An internal accuracy check of the dynamic finite element algorithm was made by computing the instantaneous energy balance of the entire system. Typical results for four crack lengths are shown in Tables 1 and 2. It is interesting to note that the accuracy of this energy balance is somewhat lower for Model No. 6 specimen which also showed larger oscillation in dynamic stress intensity factors with crack propagation.

CONCLUSIONS

A dynamic finite element algorithm has been developed for computing the dynamic stress intensity factors from experimentally determined crack position versus the relation of a propagating and arresting crack. Accuracy of the developed numerical procedure was checked by comparing the numerically determined stress intensity factors with those determined in four dynamic photoelastic experiments.

The numerically and experimentally determined dynamic stress intensity factors of two wedge-loaded DCB specimens indicate that the crack propagates under a fixed grip condition.

ACKNOWLEDGEMENT

The results of this investigation were obtained in a research contract

funded by the Office of Naval Research under Contract No. N00014-76-C-00[illegible], NR 064-478. The authors wish to acknowledge the support and encouragement of Drs. N.R. Perrone and D. Mulville of ONR during the course of this investigation.

TABLE 1 - ENERGY BALANCE IN C-DCB MODEL NO. 6

Crack Extension	W	U	K	F	(U + K + F)/W - 1
1.0	3.201	2.221	0.223	0.534	- 0.070
2.0	3.201	1.956	0.074	0.879	- 0.091
3.0	3.201	1.748	0.038	1.114	- 0.094
3.5*	3.201	1.629	0.055	1.154	- 0.113

TABLE 2 - ENERGY BALANCE IN C-DCB MODEL NO. 7

Crack Extension	W	U	K	F	(U + K + F)/W - 1
0.25	1.084	0.957	0.015	0.079	- 0.033
0.50	1.084	0.867	0.034	0.116	- 0.067
0.75	1.084	0.855	0.015	0.155	- 0.059
0.875*	1.084	0.836	0.005	0.181	- 0.062

* Crack Arrest

W: External Work
U: Strain Energy
K: Kinetic Energy
F: Fracture Energy $\equiv \int_0^c \mathcal{G}\, dc$
c: Length of Crack Extension

Unit: Pound-in.

REFERENCES

[1] Crosley, P.B. and Ripling, E.J., "Plane strain crack arrest characterizations of steels", Journal of Pressure Vessel Technology, Trans. of ASME, Vol. 97, Series J, pp. 291-298, November 1975.

[2] Burns, S.J., "Crack propagation in rapidly wedged double cantilevered beam specimens", Proc. of 12th Annual Meeting of the Society of Engineering Sciences, The University of Texas at Austin, pp. 121-129, 1975.

[3] Hoagland, R.G., Gehlen, R.C., Rosenfield, A.R. and Hahn, G.T., "The application of D.C.B. specimens for measuring the crack arrest properties of A533B and other steels", to be published in Fast Fracture and Crack Arrest, ASTM STP 627, 1977.

[4] Emery, A.F., Love, W.J. and Kobayashi, A.S., "Influence of dynamic fracture toughness on elastic crack propagation in a pressurized crack", to be published in the Proc. of the International Conference on Fracture Mechanics and Technology, Hong Kong, March 21-25, 1977.

[5] Kobayashi, T. and Dally, J.W., "The relation between crack velocity and stress intensity factor in birefringent polymers", to be published in Fast Fracture and Crack Arrest, ASTM STP 627, 1977.

[6] Kalthoff, J.F., Beinert, J. and Winkler, S., "Dynamic stress intensity factors for arresting cracks in DCB specimens", ibid loc cit.

[7] Kobayashi, A.S. and Mall, S., "Dynamic stress intensity factor of Homalite-100", presented at 1977 SESA Spring Meeting, May 16-20, 1977, Dallas, Texas.

[8] Kobayashi, A.S., Emery, A.F. and Mall, S., "Dynamic finite element and dynamic photoelastic analyses of two fracturing Homalite-100 plates", Experimental Mechanics, Vol. 16, No. 9, pp. 321-328, September 1976.

[9] Keys, S.W., "HONDO - A finite element computer program for large deformation dynamic response of axisymmetric solids", Sandia Laboratories Rep. SLA-74-0039, April 1974.

[10] Baker, B.R., "Dynamic stresses created by a moving crack", J. of Applied Mechanics, Trans. of ASME, Vol. 29, Series E, pp. 449-458, September 1962.

[11] Broberg, K.B., "The propagation of a brittle crack", Arkiv-fur-Fysik, Vol. 18, pp. 159-198, 1960.

[12] Urabe, Y., Kobayashi, A.S., Emery, A.F. and Love, W.J., "Further dynamic finite element analysis of the tapered DCB specimen", submitted for publication in Trans. of ASME.

[13] Hahn, G.T., Gehlen, P.C., Hoagland, R.G., Marschall, C.W., Kanninen, M.F., Popelar, C. and Rosenfield, A.R., "Critical experiments and analyses to establish a crack arrest methodology for nuclear pressure vessel steels", BMI-NUREG-1959, Battelle Columbus Laboratories Report, pp. 2-45-2-71, October 1976.

[14] Irwin, G.R., Dally, J.W., Kobayashi, T., Fourney, W.L. and Etheridge, J.M., "A photoelastic characterization of dynamic fracture", NUREG-0072, U.S. Nuclear Regulatory Commission, December 1976.

[15] Urabe, Y., Kobayashi, A.S., Emery, A.F. and Love, W.J., "Dynamic finite element analysis of a tapered DCB specimen", to be published in the Proc. of the International Conference on Fracture Mechanics and Technology, Hong Kong, March 21-25, 1977.

[16] Crosley, P.B. and Ripling, E.J., "Characteristics of a run-arrest segment of crack extension", to be published in Fast Fracture and Crack Arrest, ASTM STP 627, 1977.

[17] Crosley, P.B. and Ripling, E.J., "Towards development of a standard test for measuring K_{Ia}", ibid loc cit.

400 314

Administrative & Liaison Activities

Chief of Naval Research
Department of the Navy
Arlington, Virginia 22217
Attn: Code 474 (2)
471
222

Director
ONR Branch Office
495 Summer Street
Boston, Massachusetts 02210

Director
Naval Research Laboratory
Attn: Code 2629 (ONRL)
Washington, D.C. 20390 (6)

U.S. Naval Research Laboratory
Attn: Code 2627
Washington, D.C. 20390

Director
ONR - New York Area Office
715 Broadway - 5th Floor
New York, N.Y. 10003

Director
ONR Branch Office
1030 E. Green Street
Pasadena, California 91101

Defense Documentation Center
Cameron Station
Alexandria, Virginia 22314 (12)

NASA

Commanding Officer
U.S. Army Research Office Durham
Attn: Mr. J.J. Murray
CRD-AA-IP
Box CM, Duke Station
Durham, North Carolina 27706 (2)

Commanding Officer
AMXMR-ATL
Attn: Mr. R. Shea
US Army Materials Res. Agency
Watertown, Massachusetts 02172

Watervliet Arsenal
MAGOS Research Center
Watervliet, New York 12189
Attn: Director of Research

Technical Library

Redstone Scientific Info. Center
Chief, Document Section
U.S. Army Missile Command
Redstone, Arsenal, Alabama 35809

Army R&D Center
Fort Belvoir, Virginia 22060

Navy

Commanding Officer and Director
Naval Ship Research & Development Center
Bethesda, Maryland 20034
Attn: Code 042 (Tech. Lib. Br.)
17
172
174
177
1800 (Appl. Math. Lab.)
5412S (Dr. W.D. Sette)
19
1901 (Dr. M. Strassberg)
1945
196
1962

Naval Weapons Laboratory
Dahlgren, Virginia 22448

Naval Research Laboratory
Washington, D.C. 20375
Attn: Code 8400
8410
8430
8440
6300
6390
6380

Undersea Explosion Research Div.
Naval Ship R&D Center
Norfolk Naval Shipyard
Portsmouth, Virginia 23709
Attn: Dr. E. Palmer
Code 780

Naval Ship Research & Development Center
Annapolis Division
Annapolis, Maryland 21402
Attn: Code 2740 - Dr. Y.F. Wang
28 - Mr. R.J. Wolfe
281 - Mr. R.B. Niederberger
2814 - Dr. H. Vanderveldt

Technical Library
Naval Underwater Weapons Center
Pasadena Annex
3202 E. Foothill Blvd.
Pasadena, California 91107

U.S. Naval Weapons Center
China Lake, California 93557
Attn: Code 4062 - Mr. W. Werback
4520 - Mr. Ken Bischel

Commanding Officer
U.S. Naval Civil Engr. Lab
Code L31
Port Hueneme, California 93041

Technical Director
U.S. Naval Ordnance Laboratory
White Oak
Silver Spring, Maryland 20910

Technical Director
Naval Undersea R&D Center
San Diego, California 92132

Supervisor of Shipbuilding
U.S. Navy
Newport News, Virginia 23607

Technical Director
Mare Island Naval Shipyard
Vallejo, California 94592

U.S. Navy Underwater Sound Ref. Lab.
Office of Naval Research
PO Box 8337
Orlando, Florida 32806

Chief of Naval Operations
Dept. of the Navy
Washington, D.C. 20350
Attn: Code Op07T

Strategic Systems Project Office
Department of the Navy
Washington, D.C. 20390
Attn: NSP-001 Chief Scientist

Deep Submergence Systems
Naval Ship Systems Command
Code 39522
Department of the Navy
Washington, D.C. 20360

Engineering Dept.
US Naval Academy
Annapolis, Maryland 21402

Naval Air Systems Command
Dept. of the Navy
Washington, D.C. 20360
Attn: NAVAIR 5302 Aero & Structures
5308 Structures
52031F Materials
604 Tech. Library
320B Structures

Director, Aero Mechanics
Naval Air Development Center
Johnsville
Warminster, Pennsylvania 18974

Technical Director
U.S. Naval Undersea R&D Center
San Diego, California 92132

Engineering Department
U.S. Naval Academy
Annapolis, Maryland 21402

Naval Facilities Engineering Command
Dept. of the Navy
Washington, D.C. 20360
Attn: NAVFAC 0, Research & Development
04 " "
14414 Tech. Library

Naval Sea Systems Command
Dept. of the Navy
Washington, D.C. 20360
Attn: NAVSHIP 03 Res. & Technology
031 Ch. Scientist for R&D
03412 Hydromechanics
037 Ship Silencing Div.
035 Weapons Dynamics

Naval Ship Engineering Center
Prince Georges' Plaza
Hyattsville, Maryland 20782
Attn: NAVSEC 6100 Ship Sys. Engr. & Des. Dept.
6102C Computer-Aided Ship Des.
6105C
6110 Ship Concept Design
6120 Hull Div.
6120D Hull Div.
6128 Surface Ship Struct.
6129 Submarine Struct.

Air Force

Commander WADD
Wright-Patterson Air Force Base
Dayton, Ohio 45433
Attn: Code WWRMDD
AFFDL (FDDS)
Structures Division
AFLC (MCSEA)

Chief, Applied Mechanics Group
U.S. Air Force Inst. of Tech.
Wright-Patterson Air Force Base
Dayton, Ohio 45433

Chief, Civil Engineering Branch
WLRC, Research Division
Air Force Weapons Laboratory
Kirtland AFB, New Mexico 87117

Air Force Office of Scientific Research
1400 Wilson Blvd.
Arlington, Virginia 22209
Attn: Mechanics Div.

NASA

Structures Research Division
National Aeronautics & Space Admin.
Langley Research Center
Langley Station
Hampton, Virginia 23365

National Aeronautic & Space Admin.
Scientific Administrator for Advanced
Research & Technology
Washington, D.C. 02546

Scientific & Tech. Info. Facility
NASA Representative (S-AK/DL)
P.O. Box 5700
Bethesda, Maryland 20014

Other Government Activities

Commandant
Chief, Testing & Development Div.
U.S. Coast Guard
1300 E. Street, N.W.
Washington, D.C. 20226

Technical Director
Marine Corps Dev. & Educ. Command
Quantico, Virginia 22134

Director
National Bureau of Standards
Washington, D.C. 20234
Attn: Mr. B.L. Wilson, EM 219

Dr. M. Gaus
National Science Foundation
Engineering Division
Washington, D.C. 20550

Science & Tech. Division
Library of Congress
Washington, D.C. 20540

Director
Defense Nuclear Agency
Washington, D.C. 20305
Attn: SPSS

Commander Field Command
Defense Nuclear Agency
Sandia Base
Albuquerque, New Mexico 87115

Director Defense Research & Engrg.
Technical Library
Room 3C-128
The Pentagon
Washington, D.C. 20301

Chief, Airframe & Equipment Branch
FS-120
Office of Flight Standards
Federal Aviation Agency
Washington, D.C. 20553

Chief, Research and Development
Maritime Administration
Washington, D.C. 20235

Deputy Chief, Office of Ship Constrt.
Maritime Administration
Washington, D.C. 20235
Attn: Mr. U.L. Russo

Atomic Energy Commission
Div. of Reactor Devel. & Tech.
Germantown, Maryland 20767

Ship Hull Research Committee
National Research Council
National Academy of Sciences
2101 Constitution Avenue
WAshington, D.C. 20418
Attn: Mr. A.R. Lytle

PART 2 - CONTRACTORS AND OTHER TECHNICAL COLLABORATORS

Universities

Dr. J. Tinsley Oden
University of Texas at Austin
345 Eng. Science Bldg.
Austin, Texas 78712

Prof. Julius Miklowitz
California Institute of Technology
Div. of Engineering & Applied Sciences
Pasadena, California 91109

Dr. Harold Liebowitz, Dean
School of Engr. & Applied Science
George Washington University
725 23rd St. N.W.
Washington, D.C. 20006

Prof. Eli Sternberg
California Institute of Technology
Div. of Engr. & Applied Sciences
Pasadena, California 91109

Prof. Paul M. Naghdi
University of California
Div. of Applied Mechanics
Etcheverry Hall
Berkeley, California 94720

Professor P.S. Symonds
Brown University
Division of Engineering
Providence, R.I. 02912

Prof. A.J. Durelli
The Catholic University of America
Civil/Mechanical Engineering
Washington, D.C. 20017

Prof. R.B. Testa
Columbia University
Dept. of Civil Engineering
S.W. Mudd Bldg.
New York, N.Y. 10027

Prof. H.H. Bleich
Columbia University
Dept. of Civil Engineering
Amsterdam & 120th St.
New York, N.Y. 10027

Prof. F.L. DiMaggio
Columbia University
Dept. of Civil Engineering
616 Mudd Building
New York, N.Y. 10027

Prof. A.M. Freudenthal
George Washington University
School of Engineering & Applied Science
Washington, D.C. 20006

D.C. Evans
University of Utah
Computer Science Division
Salt Lake City, Utah 84112

Prof. Norman Jones
Massachusetts Inst. of Technology
Dept. of Naval Architecture & Marine Engineering
Cambridge, Massachusetts 02139

Professor Albert I. King
Biomechanics Research Center
Wayne State University
Detroit, Michigan 48202

Dr. V.R. Hodgson
Wayne State University
School of Medicine
Detroit, Michigan 48202

Dean B.A. Boley
Northwestern University
Technological Institute
2145 Sheridan Road
Evanston, Illinois 60201

Prof. P.G. Hodge, Jr.
University of Minnesota
Dept. of Aerospace Engr. & Mechanics
Minneapolis, Minnesota 55455

Dr. D.C. Drucker
University of Illinois
Dean of Engineering
Urbana, Illinois 61801

Prof. N.M. Newmark
University of Illinois
Dept. of Civil Engineering
Urbana, Illinois 61801

Prof. E. Reissner
University of California, San Diego
Dept. of Applied Mechanics
La Jolla, California 92037

Prof. William A. Nash
University of Massachusetts
Dept. of Mechanics & Aerospace Engr.
Amherst, Massachusetts 01002

Library (Code 0384)
U.S. Naval Postgraduate School
Monterey, California 93940

Prof. Arnold Allentuch
Newark College of Engineering
Dept. of Mechanical Engineering
323 High Street
Newark, New Jersey 07102

Dr. George Herrmann
Stanford University
Dept. of Applied Mechanics
Stanford, California 94305

Prof. J.D. Achenbach
Northwestern University
Dept. of Civil Engineering
Evanston, Illinois 60201

Director, Applied Research Lab.
Pennsylvania State University
P.O. Box 30
State College, Pennsylvania 16801

Prof. Eugen J. Skudrzyk
Pennsylvania State University
Applied Research Laboratory
Dept. of Physics - P.O. Box 30
State College, Pennsylvania 16801

Prof. J. Kempner
Polytechnic Institute of Brooklyn
Dept. of Aero. Engr. & Applied Mech.
333 Jay Street
Brooklyn, N.Y. 11201

Prof. J. Klosner
Polytecnic Institute of Brooklyn
Dept. of Aerospace & Appl. Mech.
333 Jay Street
Brooklyn, N.Y. 11201

Prof. R.A. Schapery
Texas A&M University
Dept. of Civil Engineering
College Station, Texas 77840

Prof. W.D. Pilkey
University of Virginia
Dept. of Aerospace Engineering
Charlottesville, Virginia 22903

Dr. H.G. Schaeffer
University of Maryland
Aerospace Engineering Dept.
College Park, Maryland 20742

Prof. K.D. Willmert
Clarkson College of Technology
Dept. of Mechanical Engineering
Potsdam, N.Y. 13676

Dr. J.A. Stricklin
Texas A&M University
Aerospace Engineering Dept.
College Station, Texas 77843

Dr. L.A. Schmit
University of California, LA
School of Engineering & Applied Science
Los Angeles, California 90024

Dr. H.A. Kamel
The University of Arizona
Aerospace & Mech. Engineering Dept.
Tucson, Arizona 85721

Dr. B.S. Berger
University of Maryland
Dept. of Mechanical Engineering
College Park, Maryland 20742

Prof. G.R. Irwin
Dept. of Mechanical Engineering
University of Maryland
College Park, Maryland 20742

Dr. S.J. Fenves
Carnegie-Mellon University
Dept. of Civil Engineering
Schenley Park
Pittsburgh, Pennsylvania 15213

Dr. Ronald L. Huston
Dept. of Engineering Analysis
Mail Box 112
University of Cincinnati
Cincinnati, Ohio 45221

Prof. George Sih
Dept. of Mechanics
Lehigh University
Bethlehem, Pennsylvania 18015

Prof. A.S. Kobayashi
University of Washington
Dept. of Mechanical Engineering
Seattle, Washington 98195

Librarian
Webb Institute of Naval Architecture
Crescent Beach Road, Glen Cove
Long Island, New York 11542

Prof. Daniel Frederick
Virginia Polytechnic Institute
Dept. of Engineering Mechanics
Blacksburg, Virginia 24061

Prof. A.C. Eringen
Dept. of Aerospace & Mech. Sciences
Princeton University
Princeton, New Jersey 08540

Dr. S.L. Koh
School of Aero., Astro. & Engr. Sci.
Purdue University
Lafayette, Indiana

Prof. E.H. Lee
Div. of Engr. Mechanics
Stanford University
Stanford, California 94305

Prof. R.D. Mindlin
Dept. of Civil Engineering
[illegible]umbia University
[illegible]. Mudd Building
[illegible] York, N.Y. 10027

Prof. S.B. Dong
University of California
Dept. of Mechanics
Los Angeles, California 90024

Prof. Burt Paul
University of Pennsylvania
Towne School of Civil & Mech. Engr.
Rm. 113 - Towne Building
220 S. 33rd Street
Philadelphia, Pennsylvania 19104

Prof. H.W. Liu
Dept. of Chemical Engineering & Metall.
Syracuse University
Syracuse, N.Y. 13210

Prof. S. Bodner
Technion R&D Foundation
Haifa, Israel

Prof. R.J.H. Bollard
Chairman, Aeronautical Engr. Dept.
207 Guggenheim Hall
University of Washington
Seattle, Washington 98195

Prof. G.S. Heller
Division of Engineering
Brown University
Providence, Rhode Island 02912

Prof. Werner Goldsmith
Dept. of Mechanical Engineering
Div. of Applied Mechanics
University of California
Berkeley, California 94720

Prof. J.R. Rice
Division of Engineering
Brown University
Providence, Rhode Island 02912

Prof. R.S. Rivlin
Center for the Application of Mathematics
Lehigh University
Bethlehem, Pennsylvania 18015

Library (Code 0384)
U.S. Naval Postgraduate School
Monterey, California 93940

Dr. Francis Cozzarelli
Div. of Interdisciplinary Studies & Research
School of Engineering
State University of New York
Buffalo, N.Y. 14214

Industry and Research Institutes

Library Services Department
Report Section Bldg. 14-14
Argonne National Laboratory
9700 S. Cass Avenue
Argonne, Illinois 60440

Dr. M.C. Junger
Cambridge Acoustical Associates
129 Mount Auburn St.
Cambrige, Massachusetts 02138

Dr. L.H. Chen
General Dynamics Corporation
Electric Boat Division
Groton, Connecticut 06340

Dr. J.E. Greenspon
J.G. Engineering Research Associates
3831 Menlo Drive
Baltimore, Maryland 21215

Dr. S. Batdorf
The Aerospace Corp.
P.O. Box 92957
Los Angeles, California 90009

Dr. K.C. Park
Lockheed Palo Alto Research Laboratory
Dept. 5233, Bldg. 205
3251 Hanover Street
Palo Alto, California 94304

Library
Newport News Shipbuilding and Dry Dock Co.
Newport New, Virginia 23607

Dr. W.F. Bozich
McDonnell Douglas Corporation
5301 Bolsa Ave.
Huntington Beach, California 92647

Dr. H.N. Abramson
Southwest Research Institute
Technical Vice President
Mechanical Sciences
P.O. Drawer 28510
San Antonio, Texas 78284

Dr. R.C. DeHart
Southwest Research Institute
Dept. of Structural Research
PO Drawer 28510
San Antonio, Texas 78284

Dr. M.L. Baron
Weidlinger Associates,
Consulting Engineers
110 East 59th Street
New York, N.Y. 10022

Dr. W.A. von Riesemann
Sandia Laboratories
Sandia Base
Albuquerque, New Mexico 87115

Dr. T.L. Geers
Lockheed Missiles & Space Co.
Palo Alto Research Laboratory
3251 Hanover Street
Palo Alto, California 94304

Dr. J.L. Tocher
Boeing Computer Services, Inc.
P.O. Box 24346
Seattle, Washington 98124

Mr. William Caywood
Code 8BE, Applied Physics Laboratory
8621 Georgia Avenue
Silver Spring, Maryland 20034

Mr. P.C. Durup
Lockheed-California Company
Aeromechanics Dept., 74-43
Burbank, California 91503

Addendum:

Assistant Chief for Technology
Office of Naval Research, Code 200
Arlington, Virginia 22217

Unclassified

SECURITY CLASSIFICATION OF THIS PAGE (When Data Entered)

REPORT DOCUMENTATION PAGE		READ INSTRUCTIONS BEFORE COMPLETING FORM
1. REPORT NUMBER TR No. 28	2. GOVT ACCESSION NO	3. RECIPIENT'S CATALOG NUMBER TR-28
4. TITLE (and Subtitle) A Procedure for Evaluating Fracture Dynamic Parameters from Crack Velocity Measurements		5. TYPE OF REPORT & PERIOD COVERED Interim Report 6. PERFORMING ORG. REPORT NUMBER
7. AUTHOR(s) A.S. Kobayashi and S. Mall		8. CONTRACT OR GRANT NUMBER(s) N00014-76-C-0060 NR 064-478
9. PERFORMING ORGANIZATION NAME AND ADDRESS University of Washington Department of Mechanical Engineering Seattle, Washington 98195		10. PROGRAM ELEMENT, PROJECT, TASK AREA & WORK UNIT NUMBERS
11. CONTROLLING OFFICE NAME AND ADDRESS Office of Naval Research Arlington, Virginia		12. REPORT DATE May 1977 13. NUMBER OF PAGES 13
14. MONITORING AGENCY NAME & ADDRESS(if different from Controlling Office)		15. SECURITY CLASS. (of this report) 15a. DECLASSIFICATION/DOWNGRADING SCHEDULE

16. DISTRIBUTION STATEMENT (of this Report)

Unlimited

17. DISTRIBUTION STATEMENT (of the abstract entered in Block 20, if different from Report)

18. SUPPLEMENTARY NOTES

19. KEY WORDS (Continue on reverse side if necessary and identify by block number)

Fracture Mechanics
Crack Propagation
Crack Arrest
Impact
Dynamic Photoelasticity

20. ABSTRACT (Continue on reverse side if necessary and identify by block number)

A combined numerical and experimental procedure for evaluating some of the fracture dynamic parameters which govern the crack run-arrest response in a fracturing plate are discussed. A dynamic finite element code is used to compute the dynamic stress intensity factor and dynamic energy release rate associated with a propagating crack which is driven by the experimentally determined crack velocity. Numerical results generated by the developed procedure are then compared with dynamic stress intensity factors obtained through dynamic photoelastic analyses of fracturing Homalite-100 plates. Two (OVER)

DD FORM 1 JAN 73 1473 EDITION OF 1 NOV 65 IS OBSOLETE
S/N 0102-014-6601

Unclassified

SECURITY CLASSIFICATION OF THIS PAGE (When Data Entered)

ABSTRACT (Continued)

edge-cracked specimens with fixed edge displacement loadings and two wedge-loaded double cantilever beam specimens were considered in this comparative study. Good agreements were obtained between the results obtained by the developed numerical-experimental procedure and dynamic photoelasticity.


DAT
ILM